The role of hydrodynamic interactions in the migration of polyelectrolytes driven by a pressure gradient and an electric field

Rahul Kekre, Jason E. Butler, and Anthony J. C. Ladd

Department of Chemical Engineering, University of Florida,

Gainesville, Florida 32611-6005, USA

(Dated: December 19, 2010)

Abstract

Experiments have shown that DNA molecules in capillary electrophoresis migrate across field lines if a pressure gradient is applied simultaneously. We suggest that this migration results from an electrically driven flow field around the polyelectrolyte, which generates additional contributions to the center-of-mass velocity if the overall polymer conformation is asymmetric. This hypothesis leads to a coarse-grained polymer model, without explicit charges, that quantitatively explains the experimentally observed migration. The simulations contradict the widely held notion that charge neutrality eliminates the effects of hydrodynamic interactions in electrically driven flows of polyelectrolytes. We predict a measurable increase in the electrophoretic velocity of a sheared polyelectrolyte that depends on chain length.

It is frequently asserted that an electric field does not generate a long-range disturbance to the flow field around a charged macroion [1, 2], thereby explaining the weak contour-length dependence of the electrophoretic mobility of DNA and other polyelectrolytes. However, the actual situation is not so simple [3, 4]; in fact there is an electrically-induced hydrodynamic interaction between charged macroions [5], which for large separations, $\boldsymbol{r}_{ij}$, is of dipolar form,

$$\boldsymbol{u}_i = \boldsymbol{\mu}^E_{ij} \cdot Q\boldsymbol{E} = \frac{\lambda_D^2 f(a/\lambda_D)}{4\pi\eta r_{ij}^3} \left(\frac{3\boldsymbol{r}_{ij}\boldsymbol{r}_{ij}}{r_{ij}^2} - \mathbf{1} \right) \cdot Q\boldsymbol{E}, \tag{1}$$

where λ_D is the Debye screening length, a and Q are the macroion radius and charge, and η is the solvent viscosity. Although the Oseen field generated by the electric force on a macroion is counterbalanced by an opposing force on the surrounding counterions, there is a residual flow from the quadrupole moment of the charge density, which gives rise to an electrophoretic analogue of the Rotne-Prager tensor, $\boldsymbol{\mu}^E_{ij}$, given by Eq. (1). In the thin double layer limit ($a \gg \lambda_D$) the hydrodynamic interaction vanishes, $f \to 0$, but for diffuse double layers ($a \ll \lambda_D$), $f \to 1$ [5]. The monomer size of DNA, $a = 0.34\,\mathrm{nm}$, is significantly less than the screening length in millimolar salt solutions, $\lambda_D \sim 10\,\mathrm{nm}$, so that the diffuse limit is appropriate in moderate to low salt conditions.

In view of Eq. (1), electrophoretically driven flows may lead to new phenomena in situations where the mean polymer conformation is aspherical. In fact, a number of experiments have shown that DNA molecules in capillary electrophoresis migrate across the field lines when a pressure gradient is applied in combination with the electric field [6–9]. Interestingly, the polymer concentrates near the wall when the pressure-gradient is applied counter to the electric field, but near the center of the capillary when the flow and field are aligned. We have previously suggested that lateral migration in capillary flow electrophoresis might be explained by hydrodynamic interactions between distant segments of the chain [10, 11]. Here we show that a coarse-grained model of a polyelectrolyte, without explicit charges but with a mobility tensor based on Eq. (1), can quantitatively account for the experimentally observed migration without any fitting parameters. Our results show that the insensitivity of the electrophoretic mobility of polyelectrolytes to variations in contour length is due to spherical averaging of the polymer conformations, rather than a complete screening of the hydrodynamic interactions. Our simulations predict that the electrophoretic mobility of a sheared polyelectrolyte will show a measurable dependence on chain length, even for large

molecular weights.

We consider a single polyelectrolyte chain in a microchannel that is 75 μm across; either parallel plates, a cylindrical tube or a square duct. It is not yet feasible to simulate a long DNA strand with explicit charges (up to 10^5 for the polymer and approximately 10^8 for the surrounding fluid), so we have adopted a coarse-grained bead-spring model [12, 13] with each bead representing a 1.06 μm segment or about 6200 base pairs. The potential parameters are taken from Ref. [14], except that here the repulsive force from the wall has been doubled, to eliminate crossings when the combination of flow and electric fields drive the polymer towards the boundary.

The mobility tensor describing the electrically-driven hydrodynamic interactions between the beads is constructed by assuming that each blob (or bead) of the coarse-grained model contains an electrically neutral but polarizable random coil of Q_b backbone charges and associated counterions; we further assume that the backbone charges are uniformly distributed throughout the blob. When an electric field is applied, each backbone charge and its surrounding ions generate a dipolar flow field according to Eq. (1) (with $Q = e$ and $f = 1$). The electrically-driven flow field around a blob of polyelectrolyte is then obtained by summing the contributions from charges within the blob. As a first approximation we neglect the distance between each monomer and the center of mass of the blob so that all the source terms appear to be at the center; this gives the correct long-range ($1/r_{ij}^3$) interaction between distant segments of the polyelectrolyte. Each blob then generates a flow field of the form of Eq. (1) with $Q = Q_b$ and $f = 1$. It is important to note that a picture of the blob as a charged particle surrounded by counterions is incorrect; the charges are distributed throughout the volume of the blob.

The charge associated with a single bead (or blob) is taken as,

$$Q_b = \frac{l_s e}{\lambda_B}, \tag{2}$$

where l_s is the contour length associated with the bead (1.06 μm) and λ_B is the Bjerrum length (0.7 nm in water). The effective charge density along the chain is about one-quarter of the bare charge density due to counterion condensation [15]. The electrophoretic mobility of the chain segment represented by a single bead is [1]

$$\mu_0^E = \left[\frac{3\pi\eta l_s}{\ln(\Delta/\lambda_D)} + \frac{l_s}{6\lambda_B} \left(\frac{1}{\mu^+} + \frac{1}{\mu^-} \right) \right]^{-1}, \tag{3}$$

where $\mu^{\pm}$ are the mobilities of the cations and anions and Δ is the spacing between charges on the DNA backbone (0.17 nm for λ-DNA). The electrophoretic velocity of a bead, $\boldsymbol{U}^E = \mu_0^E Q_b \boldsymbol{E}$, is independent of l_s.

We have simulated chain lengths from 5.3 μm (5 beads) to 42 μm (40 beads) using a standard Brownian dynamics algorithm [16],

$$\boldsymbol{r}_i(t+\Delta t) = \boldsymbol{r}_i(t) + \left[\boldsymbol{u}^0(r_i(t)) + \sum_{j=1}^{N} \boldsymbol{\mu}_{ij}(t) \cdot \left[\boldsymbol{F}_j^C(t) + \boldsymbol{F}_j^B(t)\right] + \sum_{j=1}^{N} \boldsymbol{\mu}_{ij}^E(t) \cdot Q_b \boldsymbol{E}\right] \Delta t, \quad (4)$$

to integrate the Langevin equation for the bead positions. In Eq. (4), $\boldsymbol{u}^0(\boldsymbol{r})$ is the ambient flow field, $\boldsymbol{F}^B$ is a Brownian force with variance $\left\langle \boldsymbol{F}_i^B \boldsymbol{F}_j^B \right\rangle = 2\boldsymbol{\mu}_{ij}^{-1}\Delta t$, and $\boldsymbol{F}^C$ is the sum of the conservative forces, including interactions with the confining walls.

The hydrodynamic mobility tensor, $\boldsymbol{\mu}_{ij}$, includes the self-interaction, the Rotne-Prager interaction between the beads [17], and a regularized interaction between a bead and a planar boundary [14]. In this work we use a superposition approximation to the Green's function for a confined pair of particles, which is quite acceptable when the shear rates are small [14]. The electrophoretic interaction, $\boldsymbol{\mu}_{ij}^E$, also includes reflections at the boundaries within the same superposition approximation. The self-interaction terms, $\boldsymbol{\mu}_{ii}$ and $\boldsymbol{\mu}_{ii}^E$, include both the single-particle mobilities, μ_0 and μ_0^E, and the interactions between the bead and a nearby boundary.

Lateral migration of neutral polymers is now understood to be due to hydrodynamic interactions between the polymer and the confining walls [18, 19]. In a pressure-driven flow the local shear rate stretches the polymer, which generates a net lift force from the boundary [11, 20, 21]. However, these mechanisms only act within the vicinity of the boundary, on the order of the radius of gyration, R_g, and always produce migration towards the center of the channel. Experiments on DNA in combined electric and pressure-driven-flow fields [6, 7] show significant cross-channel migration over length scales of the order of the channel dimension ($\sim 100R_g$), similar to the simulation results shown in Fig. 1. The wide channel and relatively weak fields in these experiments minimize the lift from the boundaries, and no lateral migration was observed when either the electric field or the pressure gradient were applied individually.

In Fig. 1 we show simulation results for the steady-state concentration profile of a 21 μm $\lambda-$DNA strand (20 beads) confined within a flat channel of width 75 μm ($\sim 100R_g$). The fluid is driven by a pressure gradient, $\partial_x p$, along the axial (x) direction and the polymer

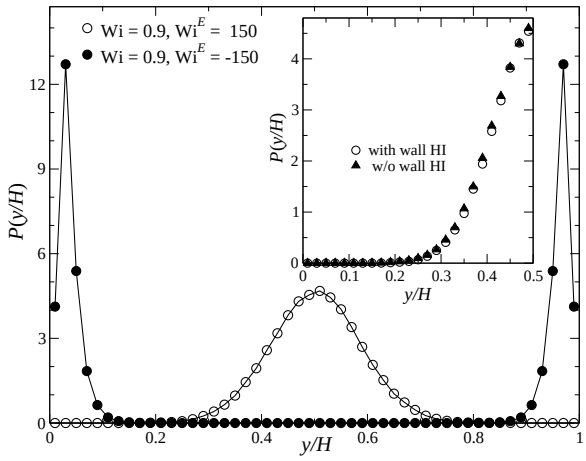

FIG. 1: Center of mass distribution for concurrent (open circles) and counter-current (solid circles) application of an external electric-field and a pressure gradient. The inset shows results with and without the contributions of the walls to the hydrodynamic interactions (lower half of the channel only).

is driven by an additional body force on each bead $Q_b E_x$. The screening length, mean shear rate and electric field were chosen to match the conditions listed in Fig. 6 of Ref. [6]: $\lambda_D = 140\,\mathrm{nm}$, $\bar{\gamma} = 4.09\,\mathrm{s}^{-1}$, and $E_x = 62.5\,\mathrm{V\,cm}^{-1}$. The shear rate is then characterized by a dimensionless Weissenberg number, $\mathrm{Wi} = \bar{\gamma}\tau = 0.9$, where τ is the viscous relaxation time of the polymer [14]. We introduce a different Weissenberg number to characterize the electrophoretic velocity, $\mathrm{Wi}^E = \mu_0^E Q_b E_x \tau / R_g = 150$. Simulations including electrically driven hydrodynamic interactions, Eq. (1), exhibit the same qualitative behavior as the laboratory experiments; the polymer migrates towards the center of the channel when the flow and electric field are aligned (concurrent), but towards the walls when they act in opposition (countercurrent). On the other hand, if the electrically-driven HI are neglected then the polymer is uniformly distributed across the channel.

Migration of polyelectrolytes in combined shear and electric fields can be understood by considering the effect of an electric field on a polyelectrolyte chain that has been distorted by a shear flow. The distribution of configurations is approximately Gaussian, $P(\boldsymbol{r}) = (2\pi|\boldsymbol{G}|)^{-3/2} \exp(-\boldsymbol{r}\cdot\boldsymbol{G}^{-1}\cdot\boldsymbol{r}/2)$, with a gyration tensor $\boldsymbol{G}(\mathrm{Wi}) = N^{-1}\sum_{i=1}^{N}\langle \boldsymbol{r}_i \boldsymbol{r}_i\rangle$; at equilibrium $\boldsymbol{G}(\mathrm{Wi}=0) = (R_g^2/3)\mathbf{1}$. In a weak shear flow, the polymer is stretched and oriented with respect to the pressure-gradient, $\delta P(\boldsymbol{r}) \sim P^{eq}(r) G_{xy} r_x r_y / R_g^4$, where $G_{xy} \propto \mathrm{Wi} R_g^2$. The electrically-driven hydrodynamic interactions then cause a cross-stream

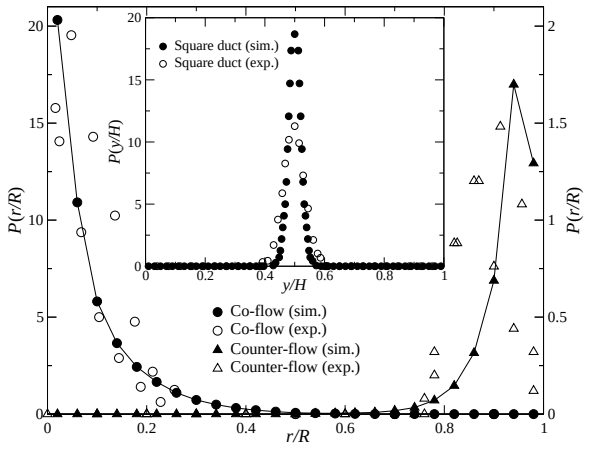

FIG. 2: Center of mass distribution for concurrent (circles) and counter-current (triangles) application of an external electric-field and pressure gradient. Simulations (solid symbols) are compared with experimental results (open symbols). The main figure compares simulations in a cylindrical cell with Fig. 6 of Ref. [6]; $\lambda_D = 140\,\mathrm{nm}$, $\mathrm{Wi} = 0.90$, $\mathrm{Wi}^E = 150$. The inset figure compares simulations in a square cell with Fig. 3 of Ref. [8]; $\lambda_D = 30\,\mathrm{nm}$, $\mathrm{Wi} = 12.5$, $\mathrm{Wi}^E = 320$. The simulation parameters were matched to the values reported for the experiments.

migration of the sheared polymer, rather like the lateral drift of a settling pair of particle, $U_y^E \sim QE_x \mathrm{Wi}\lambda_D^2/\eta R_g^2$, where $Q = NQ_b$ is the total charge on the polyelectrolyte. The direction of migration depends on the signs of the pressure gradient (via G_{xy}), and the potential gradient (via E_x).

The inset to Fig. 1 compares concentration profiles for simulations including and ignoring the effects of the confining walls on the mobilities $\boldsymbol{\mu}_{ij}$ and $\boldsymbol{\mu}_{ij}^E$. The similarity of the concentration profiles confirms that migration is dominated by the coupling between the shear rate and the electric field, and differs from what has been observed for neutral polymers [18, 22]. In fact, the small flow rate ($\mathrm{Wi} < 1$) makes the hydrodynamic lift from the walls negligible. We therefore use the mobilities for an unbounded system and match the imposed flow field to the geometry of the cell (cylindrical or square) in the corresponding experiment.

Results from a cylindrical cell are shown in Fig. 2, with parameters that were chosen to reproduce the conditions of laboratory experiments (Fig. 6 of Ref. [6]); $\lambda_D = 140\,\mathrm{nm}$, $\mathrm{Wi} = 0.90$, $\mathrm{Wi}^E = 150$. The simulated concentration profiles match the experimental data to within the statistical errors of the experiments (the statistical errors in the simulations are negligible), for both the concurrent and counter-current flows. It is significant that

there are no free parameters in these comparisons; all the constants in Eqs. (1) and (3) are determined independently. However, the electric field quoted in Ref. [6] is apparently measured across the electrodes and the field in the cell itself is not known precisely; thus the level of agreement may be fortuitous. A reasonable agreement between simulation and experiment persists down to smaller screening lengths, as shown in the inset to Fig. 2, which corresponds to 0.1mM salt [8]. In this case the glass cell was not coated with PVA (polyvinyl alcohol) and there was a significant electroosmotic flow, which is not taken into account in the simulation. Nevertheless the trends are similar, with a strong localization of polymer concentration near the center of the cell.

The extent of migration in a concurrent flow can be characterized by the concentration layer thickness, l_c, which we define as the half-width of the region encompassing 95% of the polymer concentration. In contrast to the depletion layer thickness (the distance from the boundary where there is significant polymer concentration), l_c is expected to be independent of channel width for wide channels. We explore the variation in l_c with electric field at constant pressure gradient ($\mathrm{Wi} = 0.68$) for low-salt conditions ($\lambda_D = 140\,\mathrm{nm}$). Interestingly the simulations suggest there is an optimum electric field, $\mathrm{Wi}^E \approx 10$, which maximizes the migration, as indicated by the minimum in l_c shown in Fig. 3.

The observed variation in the concentration-layer thickness is largely controlled by the response of the radius of gyration tensor, $\boldsymbol{G}$, to the increasing electric field. In a weak electric field ($\mathrm{Wi}^E < 1$) G_{xy} decreases with increasing electric field (inset to Fig. 3), suggesting that electrophoresis rotates the chain back towards the axis; however the product $G_{xy}E$ continues to increase, driving further migration towards the channel center (decreasing l_c). Nevertheless, at sufficiently high fields ($\mathrm{Wi}^E > 10$) the polymer suddenly starts to elongate to much larger dimensions, as shown by the rapid increase in $\mathrm{tr}(\boldsymbol{G})$ (inset to Fig. 3). This additional stretching further aligns the polymer with the flow direction, despite the simultaneous increase in G_{xy}, and leads to a maximum migration around $\mathrm{Wi}^E = 10$, because the hydrodynamic interactions (decaying as R^{-3}) are then spread over a larger distance.

It is well known that the electrophorectic velocity of long-chain polyelectrolytes is independent of chain length [1, 2], However, our model for a coarse-grained polyelectrolyte suggests that length-dependent electrophoresis will occur if the mean polymer configuration is non-spherical. The chain-length dependence of the electrophoretic velocity in a uniform shear flow, $u_x^0 = \gamma y$, is shown in Fig. 4 for different length DNA. In the absence

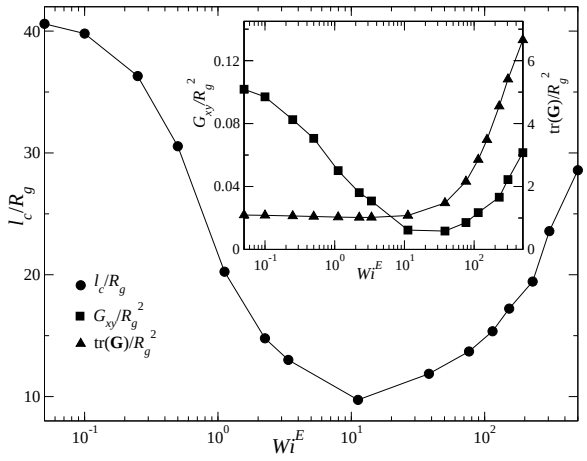

FIG. 3: Thickness of the polymer layer, l_c, for a concurrent application of electric-field and pressure-driven flow (Wi = 0.68) in a planar channel ($\lambda_D = 140\,\mathrm{nm}$). The concentration layer is taken as the half-width of the region that confines 95% of the polymer concentration (measured from the centerline). The inset to the figure shows the components G_{xy} and tr($\boldsymbol{G}$) of the radius of gyration tensor, averaged over the width of the channel. All lengths are scaled by the equilibrium radius of gyration, R_g.

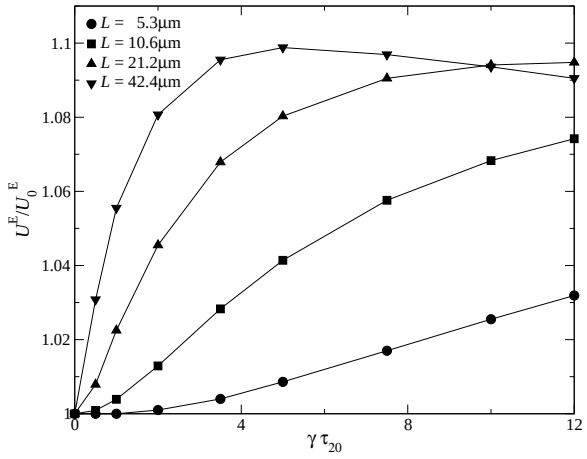

FIG. 4: Electrophoretic velocity of different length chains in a uniform shear flow, $u_x^0 = \gamma y$ ($\lambda_D = 140\,\mathrm{nm}$). The electrophoretic velocity, U^E of four different length chains are compared: $L = 5.3\,\mu$m ($N = 5$), $L = 10.6\,\mu$m ($N = 10$), $L = 21.2\,\mu$m ($N = 20$), and $L = 42.4\,\mu$m ($N = 40$). The electrophoretic velocity of the unsheared chain is U_0^E and the shear rate is non-dimensionalized by the viscous relaxation time of the 20 bead chain τ_{20}.

of flow the mobility is independent of chain length, since in this case the mean polymer conformation remains spherical. However, adding a weak shear flow stretches the polymer, $2G_{xx} - G_{yy} - G_{zz} > 0$, and then the electric field generates an additional contribution to electrophoresis from hydrodynamic interactions. The increase in the electrophoretic velocity is initially proportional to γ^2, but eventually saturates at around $1.1\mu_0^E$ when the Weissenberg number for the chain $\gamma\tau > 10$. At smaller shear rates there are measurable variations in the mobility of different length chains, possibly allowing for separation by length in a single capillary.

In this letter, we explored effects of hydrodynamic interactions in capillary electrophoresis. Our results support the contention that hydrodynamic interactions in polyelectrolytes are not completely screened by charge neutrality [3, 4]. We have shown that when electrophoresis is combined with a pressure-driven flow there is a quantitative connection between the flow field generated by the charge distribution along the extended chain and experimental observations of DNA migration. Moreover, if the polyelectrolyte is elongated by an external shear flow, there is a measurable variation in the electrophoretic velocity of different length chains. Two prediction from these simulations can be verified experimentally. First, that the electrophoretic mobility of a sheared polyelectrolyte is a function of the shear rate and chain length. Second, that there is an optimum electric field that produces the maximum migration at any give shear rate.

This work was supported by the National Science Foundation (No. CTS-0505929).

[1] G. S. Manning, J. Phys. Chem **85**, 1506 (1981).

[2] J. Barrat and J. Joanny, Adv. Chem. Phys. **94**, 1 (1994).

[3] S. A. Allison and D. Stigter, Biophys J **78**, 121 (2000), 1.

[4] D. Long and A. Ajdari, Euro Phys. J. E **4**, 29 (2001).

[5] J. Ennis and L. R. White, J Colloid Interface Sci **185**, 157 (1997).

[6] J. Zheng and E. S. Yeung, Anal. Chem. **74**, 4536 (2002).

[7] J. Zheng and E. S. Yeung, Anal. Chem. **75**, 3675 (2003).

[8] J. J. Zheng and E. S. Yeung, Aust J Chem **56**, 149 (2003).

[9] J. J. Zheng, H. W. Li, and E. S. Yeung, J Phys Chem B **108**, 10357 (2004).

[10] O. B. Usta, J. E. Butler, and A. J. C. Ladd, Phys. Rev. Lett. **98**, 098301 (2007).

[11] J. E. Butler, O. B. Usta, R. Kekre, and A. J. C. Ladd, Phys. Fluids **19**, 113101 (2007).

[12] R. M. Jendrejack, M. D. Graham, and J. dePablo, J. Chem. Phys **113**, 2894 (2000).

[13] R. M. Jendrejack, J. J. de Pablo, and M. D. Graham, J. Chem. Phys. **116**, 7752 (2002).

[14] R. Kekre, J. E. Butler, and A. J. C. Ladd, Phys. Rev. E (2010), submitted.

[15] G. S. Manning, J. Chem. Phys. **51**, 924 (1969).

[16] D. L. Ermak and J. A. McCammon, J. Chem. Phys. **69**, 1352 (1978).

[17] J. Rotne and S. Prager, J. Chem. Phys. **50**, 4831 (1969).

[18] R. M. Jendrejack, D. C. Schwartz, J. J. de Pablo, and M. D. Graham, J. Chem. Phys. **120**, 2513 (2004).

[19] D. Saintillan, E. S. G. Shaqfeh, and E. Darve, Journal of Fluid Mechanics **557**, 297 (2006).

[20] H. Ma and M. D. Graham, Phys. Fluids. **17**, 083103 (2005).

[21] C. Sendner and R. R. Netz, EPL **81**, 54006 (2008).

[22] O. B. Usta, J. E. Butler, and A. J. C. Ladd, Phys. Fluids. **18**, 031703 (2006).